Hyperfine interactions in YAB:Ho^{3+}: A high-resolution spectroscopy investigation

A. Baraldi, R. Capelletti,* and M. Mazzera
Consorzio Nazionale Interuniversitario per le Scienze Fisiche della Materia (CNISM) and Physics Department, University of Parma, Viale G.P. Usberti 7/A, Campus Universitario, 43100 Parma, Italy

N. Magnani
European Commission, Joint Research Centre, Institute for Transuranium Elements, Postfach 2340, D-76125 Karlsruhe, Germany

I. Földvári and E. Beregi
Research Institute for Solid State Physics and Optics, HAS, Konkoly-Thege ut 29-33, H-1121 Budapest, Hungary
(Received 6 July 2007; published 26 October 2007)

High-resolution spectroscopy (as fine as 0.01 cm^{-1}) was applied to a 1 mol % holmium-doped single crystal of yttrium aluminum tetraborate with the purpose of studying the hyperfine splitting of Ho^{3+} energy levels of interest for possible quantum manipulation media. The hyperfine structure was clearly revealed for a high number of lines in a wide wave number range (up to $\simeq$21 300 cm^{-1}) and for a large number of multiplets. Several different hyperfine patterns were monitored, differing in the number of lines, in their separation, and in their relative statistical weight. These features were all understood by a crystal-field model, whose results are in very good agreement with experiments and account for the involved level symmetry, the type of transitions (electric and magnetic dipole allowed), the possibility of a second-order (pseudoquadrupolar) hyperfine coupling between close levels, and a slight distortion of the local D_3 symmetry in Ho-occupied sites.

DOI: 10.1103/PhysRevB.76.165130 PACS number(s): 31.30.Gs, 42.70.Hj, 71.70.Ch, 78.30.Am

I. INTRODUCTION

According to Abragam and Pryce in their pioneering work dealing with paramagnetic resonance, "the nuclear hyperfine structure, i.e., the splitting of the lines by the action of the nucleus of the ion, though present when the spin of the nucleus differs from zero, is not normally resolved. The line breadth can be substantially reduced by working at low temperatures using magnetically diluted crystals."[1] Thus, under favorable conditions, paramagnetic resonance can supply information about hyperfine splitting of the ground electronic levels, while optical techniques allow us to analyze the hyperfine structure (hfs) of the excited states too, both for neutral configurations[2] and for ions in solids. The interest in such topics has recently been revived, as several rare-earth-doped compounds with strong hyperfine interactions have been proposed as possible quantum manipulation media[3,4] after the discovery of simultaneous tunneling of the electronic and nuclear momenta in Ho-doped $LiYF_4$.[5] Some specific isotopes of rare earths (RE), such as ^{141}Pr, ^{151}Eu, ^{153}Eu, ^{159}Tb, ^{165}Ho, and ^{169}Tm doped into crystals, are good candidates for the spectroscopic investigation of the hfs of ions embedded in a solid matrix, since they are endowed with a nuclear magnetic momentum. Moreover, the optical absorption and emission lines are expected to be very narrow (at low temperatures) because they are originated by electronic transitions within the well-shielded $4f$ shell: as a matter of fact, the hyperfine (hf) interaction depends both on the nuclear spin I and on the electronic total angular momentum J,[6] being expressed as

$$H_{hf} = A_J \mathbf{J} \cdot \mathbf{I} \tag{1}$$

within a single manifold, where A_J is the hyperfine coupling constant for the considered multiplet.[7] Among the above mentioned ions, ^{165}Ho offers the best premises for a successful hfs analysis since it has the highest nuclear ($I=7/2$) spin among rare earths and a natural abundance of 100%. In addition to this, all the low-lying manifolds of Ho^{3+} are characterized by high J (up to $J=8$ for the ground state),[8,9] thus they are expected to display relatively large hyperfine separations. In most cases, the hyperfine structure of energy spectra can be well understood by considering H_{hf} as a perturbation acting on degenerate electronic states. As the ion is embedded in a crystalline environment, the crystal field probed by Ho^{3+}, a $4f^{10}$ non-Kramers ion, may split each $^{2S+1}L_J$ manifold into several sublevels or Stark components (up to $2J+1$). The first-order approximation simply describes an effective magnetic field $A_J\langle \mathbf{J} \rangle$, which acts on the nuclear spin $\mathbf{I}$ and produces a Zeeman-like splitting. However, low-symmetry crystal fields (as, for example, those in monoclinic or rhombic crystals) may lift the manifold degeneracy completely. For nondegenerate states, the hyperfine splitting is forbidden in the first-order approximation by time reversal symmetry, and thus, is not observed.[10,11] The spectroscopic evidence of hfs related to Ho^{3+} centers is reported indeed for $LiYF_4$ (tetragonal symmetry, point group S_4),[10,12–15] CaF_2 (different centers with tetragonal, trigonal, and cubic symmetries, respectively),[16–22] and $CsCdBr_3$ (dimer center with C_v symmetry[23]): in all cases, the crystal-field symmetry is not low enough to remove completely the manifold sublevel degeneracy.

In the present work, the crystalline yttrium aluminum tetraborate, $YAl_3(BO_3)_4$ (YAB), is chosen as a host to investigate the Ho^{3+} hfs for the following reasons:

(a) YAB belongs to the trigonal system with space group $R32$, Ho^{3+} substitutes Y^{3+} in a prismatic trigonal site and experiences a D_3 crystal field,[24] therefore hfs may be observed since the manifold degeneracy cannot be completely removed by the crystal field.[25]

(b) The Y^{3+} site is the only one which can be occupied by RE^{3+} in YAB, as already supported by the theoretical analysis of the crystal-field spectra, for example, in the case of Er- and Dy-doped YAB.[25] In principle, Al^{3+}, too, might be substituted by a RE^{3+}; however, the related probability is negligible due to the large ionic radii difference.

(c) The substitution of Ho^{3+} for homovalent Y^{3+} does not require any charge compensation; therefore, only a single Ho center is expected to occur. This makes more straightforward and unequivocal the interpretation of the complex spectra. The lines induced by a given Ho center, as reported in the literature,[16,17,20–23] are indeed univocally identified in the spectra; however, the simultaneous presence of different Ho centers introduces, as a rule, additional long range disorder. This would cause inhomogeneous line broadening, i.e., a detrimental factor for resolving the hfs. Furthermore, in YAB the large separation of Y^{3+} (and, consequently, of Ho^{3+}) sites, due to the borate group interposition,[24] prevents the interaction among different Ho ions (at least for not too high RE concentrations), supporting a single Ho^{3+} environment.

(d) Besides the above mentioned basic advantages for hfs analysis, $YAB:RE^{3+}$ is a family of promising nonlinear materials in the field of integrated optical applications. The RE radiative transitions may be exploited to tailor solid state lasers, and the large nonlinear optical coefficients coupled to a wide transparency window may allow laser frequency doubling (self-frequency doubling).[26] The Ho^{3+} doping provides an attractive 2 μm emission, well suitable for eye-safe laser applications, in addition to other stimulated emission transitions.[8,27]

(e) At least to our knowledge, in the literature there is no detailed spectroscopic analysis of Ho^{3+} in YAB, except for room temperature fluorescence spectra in the visible and near infrared,[28] and our recent preliminary high-resolution absorption measurements.[29]

The spectroscopic analysis of $YAB:Ho^{3+}$ has been performed by applying high-resolution (as fine as 0.01 cm^{-1} nonapodized resolution) Fourier transform absorption spectroscopy in a wide wave number range (4000–25 000 cm^{-1}) and in the temperature range of 9–300 K. The doping level chosen, i.e., 1% Ho/Y molar ratio, is a reasonable compromise between two opposite requirements: to work with a *magnetically diluted crystal*, according to Abragam and Pryce,[1] and to measure the Ho^{3+} spectra with a good signal-to-noise ratio. As a matter of fact the spectral lines in crystals doped with very low RE concentrations are extremely narrow due to a reduced inhomogeneous broadening,[13,30] a necessary premise to unveil and analyze the hfs; however, this advantage is nullified if the RE lines are too weak, and thus, affected by noise. The first step was to attribute the large number of lines detected in the spectra to the transitions between the sublevels of the ground $^5I_8$ to those of the excited $^5I_7$, $^5I_6$, $^5I_5$, $^5I_4$, $^5F_5$ $^5S_2$, $^5F_4$, $^5F_3$, $^5F_2$, $^5K_8$, and $^5G_6+^5F_1$ manifolds, respectively. The experimental data were fitted by a single ion Hamiltonian, and the crystal-field parameters were obtained.[25,29,30] In addition, the symmetry of the wave functions related to each sublevel was identified. On this basis, the hfs, which was monitored for many of the observed lines, could be analyzed thanks to the small linewidths observed with high resolution at low temperature. The spectra were found to display a variety of different hyperfine splitting patterns, which were accounted for in terms of electric- and magnetic-dipole allowed transitions and interaction between rather close sublevels.

II. EXPERIMENTAL DETAILS

YAB single crystal was grown by means of the top-seeded solution growth method from a $K_2O/MoO_3/B_2O_3$ flux. Ho was added as holmium oxide (Ho_2O_3). Detailed description of the experimental conditions can be found in Ref. 31. The Ho concentration within the crystal, expressed in molar fractions (m.f.), was monitored by atomic absorption analysis and was found to be close to the nominal one (1 mol %). The crystal was x-ray oriented, cut, and polished for spectroscopic investigations. The sample, about 2 mm thick, was oriented perpendicular to the z axis. The optical absorption spectra were measured by a Bomem DA8 Fourier transform spectrophotometer in the range 4000–25 000 cm^{-1} with a nonapodized resolution as good as 0.01 cm^{-1}. The sample temperature was varied in the range 9–300 K by mounting the sample in a 21SC model Cryodine Cryocooler of CTI Cryogenics equipped with KRS5 and quartz windows. Thanks to the high-resolution spectroscopy applied at low temperature, traces of unwanted impurities, such as Cr^{3+}, were detected by monitoring the two lines (R1 and R2) originated by the $^4A_2 \rightarrow {}^2E$ crystal-field transition.[32] Traces of other rare-earth ions were unveiled as well: a specific rare earth was identified by comparing the present spectra with those of intentionally doped samples. The weak lines observed at 6526.52, 6560.82, 10 209, 10 230.1, 10 300.8, and 10 311.4 cm^{-1} were attributed to transitions from the ground $^4I_{15/2}$ to the excited $^4I_{13/2}$ and $^4I_{11/2}$ manifolds of Er in YAB.[25] Evidence for the presence of Dy^{3+} ions was revealed by the 7692.2, 7710.8, 7736.0, 7753.7, 7756.8, and 7718 cm^{-1} lines belonging to Dy^{3+} $^6H_{9/2} \rightarrow {}^6H_{9/2}+{}^6F_{11/2}$ transition.[25] A very low concentration of Yb^{3+} is also present in the sample, as revealed by the lines at 10 187.4 and 10 248.7 cm^{-1}.[33] Since no calibration is needed for the present experiment, the unwanted impurity concentration was only roughly estimated[30] and, for example, the Er^{3+} doping was evaluated to be lower than 3×10^{-2} mol %.

III. EXPERIMENTAL RESULTS

Two examples of the absorption spectra, measured in the 4000–25 000 cm^{-1} range and originated by the transitions from the ground $^5I_8$ to the excited $^5I_7$, $^5I_6$ $^5I_5$, $^5I_4$, $^5F_5$, $^5S_2$, $^5F_4$, $^5F_3$, $^5F_2$, $^5K_8$, and $^5G_6+^5F_1$ manifolds, are displayed in Figs. 1 and 2 in the 5075–5275 ($^5I_8 \rightarrow {}^5I_7$) and 15 355–15 600 cm^{-1} ($^5I_8 \rightarrow {}^5I_5$) spectral ranges, respectively. In the low wave number side of the 9 K spectrum portrayed in Fig. 1(c), very narrow lines [half maximum full width (HMFW) of 0.04 cm^{-1}] give rise to a *very fine structure*, while those at wave numbers higher than 5150 cm^{-1} show smooth profiles. Thanks to the high resolution and line sharpness, the components of the very fine structure appear well resolved in the expanded presentation covering the 5083–5093 and 5095–5105 cm^{-1} ranges, respectively [Figs. 1(a)

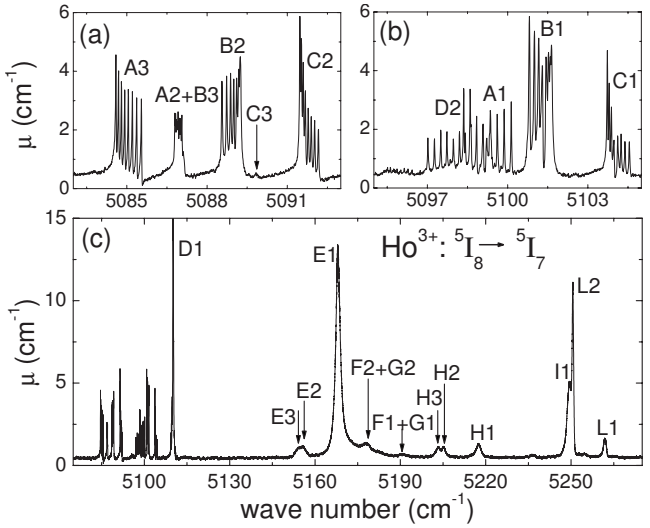

FIG. 1. Optical absorption spectrum measured at 9 K for a Ho-doped YAB sample. The whole region of Ho^{3+} $^5I_8 \rightarrow {}^5I_7$ transition is displayed: (a) 5083–5093 cm^{-1}, (b) 5095–5105 cm^{-1}, and (c) 5075–5275 cm^{-1}. The spectrum is measured with a nonapodized resolution as good as 0.01 cm^{-1}.

and 1(b)]. For example, the structure at about 5085 cm^{-1}, which spans over 1 cm^{-1}, exhibits eight components, as expected for a hyperfine structure due to Ho^{3+} endowed with a nuclear spin $I=7/2$ (see Sec. IV B). The hfs is detected for various Stark components within different $^5I_8 \rightarrow {}^{2S+1}L_J$ transitions (see Sec. IV B and Table I) in the 9 and 20 K spectra, while at 40 K, it is no longer detectable: compare, for example, curves a and b in Fig. 2, where the spectra related to the $^5I_8 \rightarrow {}^5I_5$ transition and measured at 9, 40, and 150 K are displayed. The hfs vanishing at temperatures as low as 40 K is a consequence of line broadening, which causes the merging of the very narrow hfs components which are separated at 9 K only by about 0.1 cm^{-1}. The 9 K high-resolution spectra show different hfs patterns: the most representative of them are summarized in Figs. 3 and 4, and discussed in Sec. IV B. The temperature affects deeply the spectra: by increasing the temperature, the lines also shift, their amplitude changes, and new lines appear. The last two features, which are portrayed in Fig. 2, represent one of the keys to unravel the complex spectra and build the Ho^{3+} level scheme (see Sec. IV A). As a matter of fact, by increasing the temperature, the excited sublevel population in the ground manifold increases at the expense of the lowest sublevel one. For example, by increasing the temperature from 9 to 40 K, the 15 398.6 cm^{-1} line decreases significantly, while the 15 385.4 cm^{-1} one grows [compare curves a and b in Fig. 2(a)]. At 150 K, the lines are broad, weak, and overlap [see curves c in Figs. 2(a)–2(c)]. Furthermore, additional lines appear by increasing the temperature, compare, for example, curves a–c in Fig. 2(b).

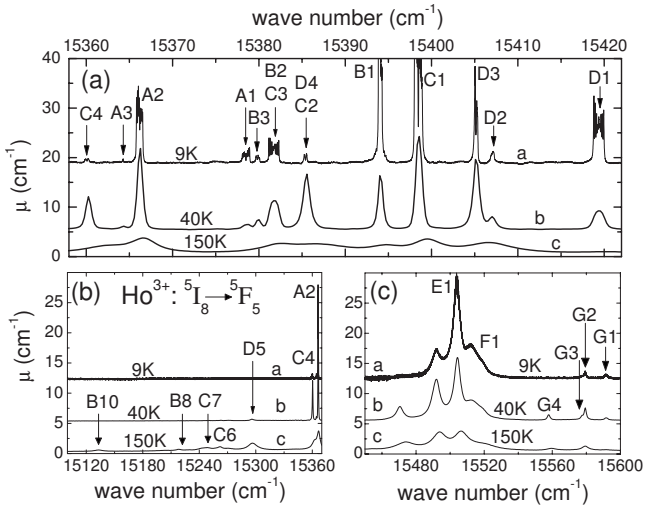

FIG. 2. Optical absorption spectra measured at different temperatures for a Ho-doped YAB sample. Curves a, 9 K, nonapodized resolution=0.01 cm^{-1}; curves b, 40 K, resolution=0.5 cm^{-1}; and curves c, 150 K, resolution=0.5 cm^{-1}. The three panels cover the whole region of Ho^{3+} $^5I_8 \rightarrow {}^5F_5$ transition: (a) 15 355–15 425 cm^{-1}, (b) 15 100–15 375 cm^{-1}, and (c) 15 450–15 600 cm^{-1}.

IV. DISCUSSION

A. Energy levels and wave function symmetry

The energy-level scheme and the correct attribution of the lines originated by the $^5I_8 \rightarrow {}^5I_7$, $^5I_6$, $^5I_5$, $^5I_4$, $^5F_5$, $^5S_2$, $^5F_4$, $^5F_3$, $^5F_2$, $^3K_8$, and $^5G_6+{}^5F_1$ transitions were obtained by following the procedure illustrated in detail in Ref. 30, i.e., by (i) measuring the absorption spectra as a function of temperature and (ii) fitting the experimental energy levels with a single-ion Hamiltonian model. At high temperatures, the intensities of the lines associated with transitions starting from the zero sublevel of the $^5I_8$ ground manifold gradually decrease, while those arising from nonzero sublevels increase and become dominant (see Fig. 2). In the present case, the line attribution is made more difficult due to the hfs overlapping for the spectra monitored at 9 and 20 K (see Figs. 1 and 2); however, it was possible to identify nearly all the X1 transitions (corresponding to the X1 lines), i.e., those starting from the lowest sublevel of the ground manifold to the sublevels of the excited $^{2S+1}L_J$ manifold (see Table I). The lines (and transitions) are labeled by Xn, where $n=1,2,3,\ldots$ indicates the ground manifold sublevel (initial state of the absorption transition) and $X=\mathrm{A},\mathrm{B},\mathrm{C},\ldots$ indicates the sublevel within a given excited manifold (final state) (see Table I). Examples are the A3, E1, and L2 lines displayed in Fig. 1. The Stark splitting of the $^5I_8$ ground state was derived by comparing the 9 K spectra to the 20, 40, and 150 K ones. Thanks to the line sharpness at low temperatures and weak line overlapping on the low energy side of the 150 K spectra, 11 sublevels could be identified (Table I). Among these, the first three are separated by only 12.26±0.35, 14.33±0.76, and 34.97±0.62 cm^{-1} from the lowest sublevel, respectively. The sublevel positions were determined by averaging a large number of *separations* related to different lines and different manifolds. For example, the 12.26±0.35 cm^{-1} figure was obtained by averaging 87 separations between X1 and X2 lines. The first three excited sublevels in the ground manifold are thermally populated even at 9 K, as proved, for example, by the weak absorptions, labeled as C4, A3, and D2 in Fig. 2(a),

TABLE I. Sublevel positions (cm^{-1}) for different manifolds $^{2S+1}L_J$ (first column) of Ho^{3+} in YAB, as derived from high-resolution absorption spectra measured at 9 K. The experimental data are compared to the calculated ones (in third and fourth columns, respectively). Γ is the symmetry of the wave function related to each sublevel. Each sublevel is labeled by i in the second column with either a number or a letter (see Sec. IV A for details). The Δ_{hf} (cm^{-1}) between the hfs components is given as the overall splitting of a given electronic sublevel: the experimental values Δ_{hf}^{exp} are compared to the calculated ones Δ_{hf}^{th} (in sixth and seventh columns, respectively). Some Δ_{hf}^{exp} could not be measured due to the broadness of the related lines.

$^{2S+1}L_J$	i	Level (expt)	Level (th)	Γ	Δ_{hf}^{exp}	Δ_{hf}^{th}
$^5I_8$	1	0	0.3	E	0.82	0.80
	2	12.26	12.8	E	0.69	0.69
	3	14.33	13.3	A_1		
	4	34.97	33.6	A_2		
	5	126	121.8	A_1		
	6	136	139.3	E		1.04
	7	148	149.2	E		0.74
	8	175	177.2	A_2		
	9	211	214.5	E		0.36
	10	262	263.5	E		0.22
	11	283	283.2	A_1		
$^5I_7$	A	5099.2	5093.2	E	0.96	0.93
	B	5101.4	5097.5	A_2	0.15[a]	0.1[a]
	C	5104	5101.1	A_1	0.14[a]	0.1[a]
	D	5110.1	5106.2	E	0.92	0.86
	E	5168	5166.7	A_2		
	F		5175.1	E		1.29
	G	5190.8	5188	A_1		
	H	5217.5	5214.6	E		0.42
	I	5248.9	5247.2	E		0.23
	L	5262	5260	A_2		
$^5I_6$	A	8595.6	8596.1	E	1.11	1.08
	B	8618	8616.6	E	0.88	0.86
	C	8637	8641.2	A_1		
	D		8644.1	A_2		
	E	8664.2	8675	A_1		
	F	8697.8	8681.5	A_2		
	G	8701.4	8701.9	E		0.43
	H	8725.8	8731.6	E		0.21
	I	8740.7	8744.8	A_1		
$^5I_5$	A	11168	11165.2	E	1.04	1.02
	B	11191	11199	A_1		
	C	11203.6	11203.6	E		1.16
	D	11204.9	11205.3	A_2		
	E	11241.3	11248.3	E		0.62
	F	11267.2	11276.3	E		0.24
	G	11282.1	11291.6	A_2		
$^5I_4$	A	13191	13186.2	A_1		
	B	13210	13213.8	E		0.0
	C	13255	13250.1	A_2		
	D		13263.5	E		0.38
	E	13373	13382.9	E		0.0

TABLE I. (*Continued.*)

$^{2S+1}L_J$	i	Level (expt)	Level (th)	Γ	Δ_{hf}^{exp}	Δ_{hf}^{th}
	F	13417	13435.8	A_1		
$^5F_5$	A	15378	15364.6	A_2		
	B	15394	15374.7	E	0.40	0.34
	C	15398.6	15388.7	A_1		
	D	15419	15417.2	E	0.25	0.23
	E	15504	15512.9	E		0.31
	F	15528	15527.5	A_2		
	G	15591.6	15590.8	E		0.76
$^5S_2$	A	18373.2	18372.6	A_1		
	B	18390.2	18385.8	E	0.10	0.05
	C	18403.2	18398.1	E		
$^5F_4$	A	18482.7	18487.5	A_1		
	B	18487	18488.2	E		0.13
	C	18517.7	18517.1	E		0.0
	D	18554.2	18559.8	A_1		
	E	18578.6	18571.8	E		0.61
	F	18583.8	18577.3	A_2		
$^5F_3$	A	20470.6	20455	A_2		
	B	20552	20553.5	E	0.09	0.13
	C	20592.5	20584.3	A_1		
	D	20629.1	20635.7	A_2		
	E	20641	20638.5	E		0.31
$^5F_2$	A	20972	20986.9	A_1		
	B	21027.6	21032.2	E		
	C	21092.4	21109.9	E		
$^3K_8$	A	21290.6	21278.5	A_1		
	B	21297	21287.2	E	0.25	0.26
	C	21313	21307.5	E	0.26	0.25
	D	21323.7	21322.9	A_2		
	E	21329	21333.4	E	1.27	0.96
	F	21342	21336.6	A_2		
	G	21357.8	21343.1	A_1		
	H	21368.5	21378	E		0.18
	I		21384.4	E		0.14
	L	21373.9	21385.4	A_1		
	M	21383.1	21390.3	E		0.48
$^5G_6+^5F_1$	A	21941	21955	A_1		
	B	21951	21963.8	A_2		
	C	21986	22003.1	A_1		
	D	21991	22004.3	E		
	E	22045	22048.4	E		
	F	22184	22174.2	A_2		
	G	22211	22199.6	A_1		
	H	22223	22225.8	E		
	I		22227.9	A_2		

TABLE I. (*Continued.*)

$^{2S+1}L_J$	i	Level (expt)	Level (th)	Γ	Δ_{hf}^{exp}	Δ_{hf}^{th}
	L	22254	22237.7	*E*		
	M	22315	22301.7	*E*		

[a]Non-equi-spaced (pseudoquadrupolar) hfs observed and calculated.

curve a. Their intensities increase by increasing the temperature [compare, for example, the amplitudes of the 15 360 and 15 385.4 cm^{-1} lines, as portrayed by curves a and b in Fig. 2(a), related to 9 and 40 K, respectively]. In YAB, a relatively large gap exists between the first four sublevels and the following seven sublevels in the ground manifold. Notwithstanding the complexity added by hfs to the absorption spectra and the incomplete lifting of the level degeneracy (see below), it was possible to identify clearly 11 sublevels in the ground manifold, i.e., a number larger than those recently reported for Ho^{3+} in bismuth tellurite and BaY_2F_8.[11,34]

The experimental energy levels were fitted with a single-ion Hamiltonian that accounts for free-ion and crystal-field interactions. The Hamiltonian which describes the $4f^{10}$ configuration of Ho^{3+} ions can be separated into several terms:

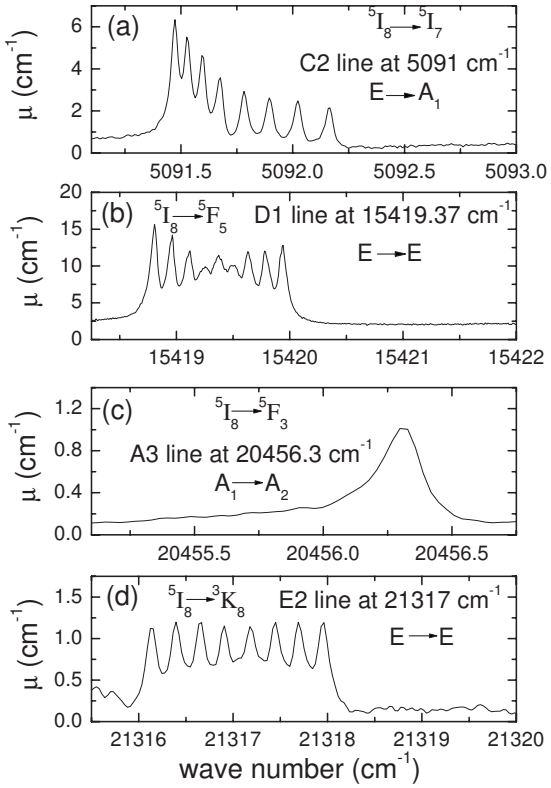

FIG. 3. Examples of hfs patterns displayed by absorption lines in different wave number ranges. (a), (b), (c), and (d) are related to lines originated within different transitions, i.e., from the ground $^5I_8$ to the excited $^5I_7$, $^5F_5$, $^5F_3$, and $^3K_8$, respectively. The spectra are measured at 9 K with a nonapodized resolution of 0.01 cm^{-1} for spectra of (a) and (b), and 0.05 cm^{-1} for those of (c) and (d), respectively.

$$H = H_{FI} + H_{CF} + H_{hf} \tag{2}$$

where the purely electronic part is limited to the free-ion (FI) and crystal-field (CF) interactions. The former, following the notation of Refs. 35 and 36, can be written as

$$H_{FI} = E_{av} + \sum_k F^k + \zeta H_{SO} + \alpha L(L+1) + \beta G(G_2) + \gamma G(R_7) + \sum_i T^i t_i + \sum_j M^j m_j + \sum_k P^k p_k, \tag{3}$$

where E_{av} represents a spherically symmetric one-electron contribution, whose variation gives rise to an energy shift of the whole configuration. The CF Hamiltonian for D_3-symmetry sites contains six nonzero parameters:

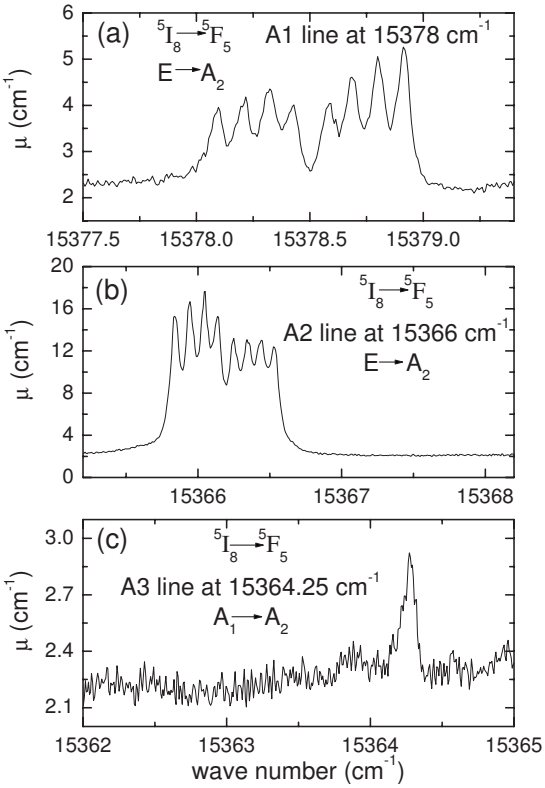

FIG. 4. Examples of hfs patterns displayed by absorption lines starting from the first three sublevels (E, E, and A_1) of the ground manifold $^5I_8$ to the same sublevel (A_2) of the $^5F_5$ excited state. The spectra are measured at 9 K with a nonapodized resolution as good as 0.01 cm^{-1}.

TABLE II. Free-ion and crystal-field parameters obtained for Ho^{3+} in YAB. The parameters whose values are given in square brackets were kept fixed during the fitting procedure (see Sec. IV A for details). The resulting rms deviation (σ) is also indicated.

Parameter	Value (cm^{-1})
E_{av}	48288±7
F_2	93675±60
F_4	66430±110
F_6	51767±60
ζ	2140.8±0.6
α	[17.15]
β	[−607.9]
γ	[1800]
T_2	[400]
T_3	[37]
T_4	[107]
T_6	[−264]
T_7	[316]
T_8	[336]
M_0	[2.54]
M_2	[1.42]
M_4	[0.79]
P_2	[605]
P_4	[302.5]
P_6	[60.5]
B_2^0	491±25
B_4^0	−1150±40
B_6^0	327±28
B_4^3	−797±31
B_6^3	−62±31
B_6^6	−162±25
σ (rms)	8.9

$$H_{CF} = \sum_{k=2,4,6} B_k^0 C_0^{(k)} + \sum_{j=4,6} B_j^3 (C_{-3}^{(j)} - C_3^{(j)}) + B_6^6 (C_{-6}^{(6)} - C_6^{(6)}); \quad (4)$$

the tensor operators $C_q^{(k)}$ are defined in Ref. 37. All the electronic energy levels listed in Table I were included in the fitting procedure and, while all six CF parameters were freely varied, 15 of the 20 free-ion coefficients (those between square brackets in Table II) were kept fixed in order to avoid overparametrization. The starting parameters for the fit were taken as those of Ho:LaF_3 for the free-ion part,[35] and Dy:YAB for the CF.[25] The relatively small value of the obtained rms deviation σ (also given in Table II) is a proof of the good quality of the fit, and the fact that the sign and order of magnitude of all CF parameters correspond to those of Dy and Er in the same material points toward a unified CF picture for YAB.[25] The theoretical assignment of level symmetry (indicated under Γ heading in Table I) corresponds to the expected allowed transition rules (Table III; no forbidden $A_1 \rightarrow A_1$ or $A_2 \rightarrow A_2$ lines were detected). As expected for D_3 symmetry, the sublevel degeneracy is not completely lifted, as proved by the presence of E doublets (Table I).

TABLE III. Selection rules for transitions between crystal-field levels in D_3 symmetry: *e*, electric-dipole allowed; *m*, magnetic-dipole allowed; and dash, forbidden.

Initial state	Final state		
	E	A_1	A_2
E	e,m	e,m	e,m
A_1	e,m	—	e,m
A_2	e,m	e,m	—

B. Hyperfine structure

Lines split by the hyperfine interaction were monitored at 9 K in all spectral ranges investigated: a few examples are displayed in Figs. 3 and 4 within the $^5I_8 \rightarrow {}^5I_7$, $^5F_5$, $^5F_3$, and $^3K_8$ transitions. By increasing the energy of the excited level reached by the absorption transition, the linewidth of the hfs components increases due to the excited state lifetime shortening. As a consequence, the wave number range covered by a given hfs broadens: for low energy lines, the hfs spans over less than 1 cm^{-1}, [see Fig. 3(a)], while for the high energy lines, it covers more than 2 cm^{-1} [see Fig. 3(d)]. In many cases, the hfs is either blurred or no longer detectable. For absorptions which show clearly resolved hfs, different patterns can be distinguished: (i) eight components [see Figs. 3(a), 3(d), 4(a), and 4(b)]; (ii) nine components [see Fig. 3(b)]. In the last case, it is more correct to say that a ninth component overlaps (in the middle) with the *standard* eight components. A hint of the ninth component can be envisaged also in Fig. 3(d) in the middle of the eight components. Moreover, the hfs components may be either evenly spaced [see Figs. 3(d) and 4(b)] or not [see Figs. 3(a), 3(b), and 4(a)]. A gap may separate into two groups the eight components [see Figs. 4(a) and 4(b)]. In addition, within a given hfs, the eight components may be either of equal [see Fig. 3(d)] or different amplitude [see Figs. 3(a), 3(b), 4(a), and 4(b), respectively]. In addition to hfs patterns, single narrow lines (HMFW of 0.2 cm^{-1}) are detected [see Figs. 3(c) and 4(c)]. The detailed analysis of all monitored patterns shows that the single narrow line appears for transitions between singlet states (A_1 and A_2), the eight components arise from transitions involving at least a doublet state (E), and the addition of a ninth component may occur for transitions connecting two E states. Figure 4 is a clear example of different hfs patterns displayed for A1, A2, and A3 lines (within $^5I_8 \rightarrow {}^5F_5$), originated by transitions starting from different initial states (E, E, and A_1) and reaching the same final state (A_2), according to the scheme of Fig. 5(a). This complex picture arises naturally when one considers the transition mechanism between two electronic levels split by the hyperfine interaction. As a first-order approximation, Eq. (1) can be written as

$$H_{hf} = -\boldsymbol{\mu}_i \cdot \mathbf{H}_0, \quad (5)$$

where μ_i is the magnetic moment of the nucleus and $\mathbf{H}_0$ is a

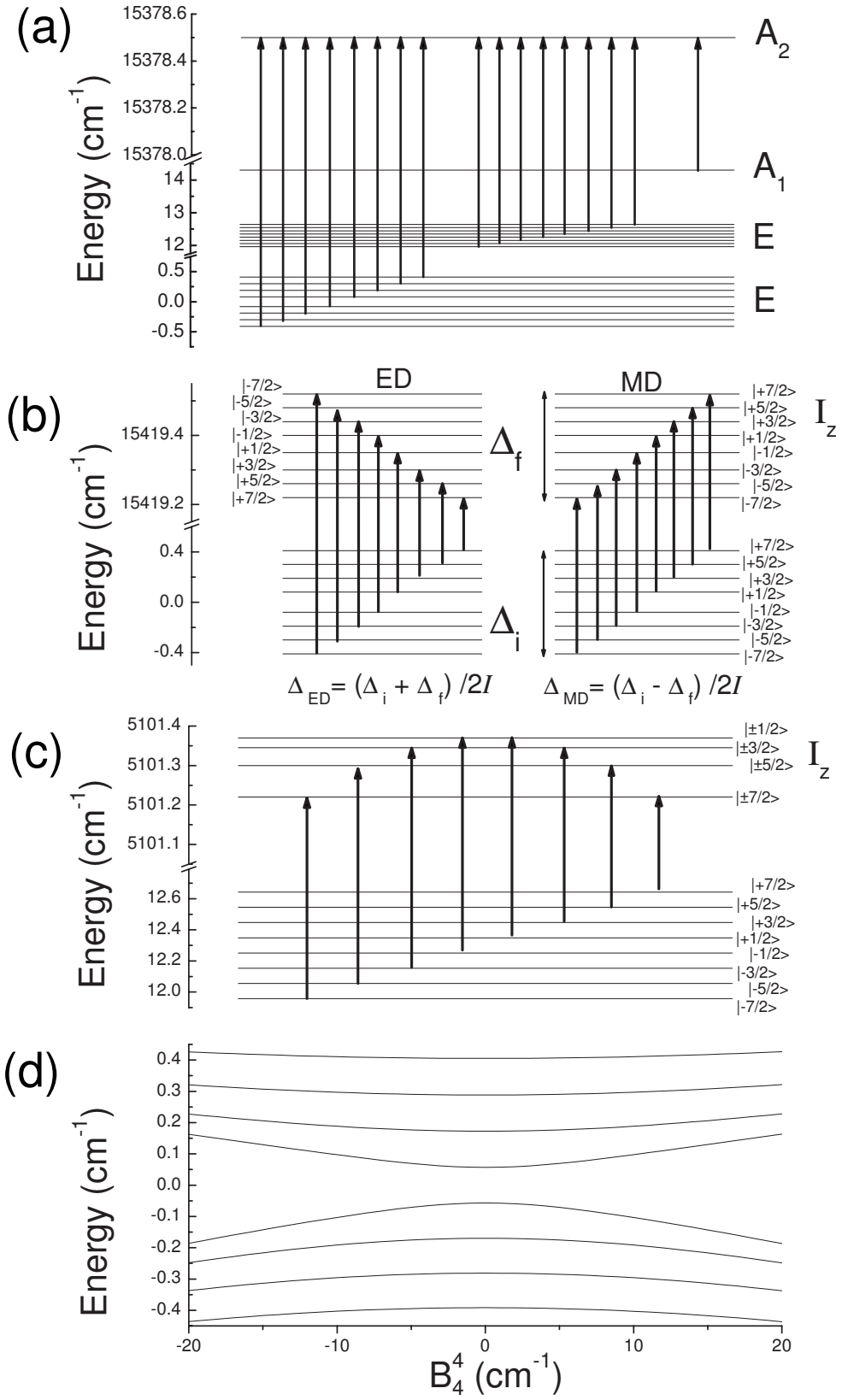

FIG. 5. [(a)–(c)] Examples of transitions originating different hfs patterns portrayed in Figs. 3 and 4: (d) shows the hyperfine splitting of the ground state as a function of B_4^4 parameter.

magnetic field created at the ion's nucleus by electrons in a given state. In this framework, the hyperfine field splits each E electronic doublet into eight equally spaced components ($I_z=-7/2,\ldots,+7/2$), while it does not affect the A_1 and A_2 singlets. A transition between two A-type levels will then result in a single line being observed, such as the A1 → A2 transition depicted in Figs. 3(c) and 4(c). Transitions between E- and A-type levels should result in the observation of eight equispaced lines, such as in Figs. 3(d) and 4(b), due to the selection rule $\Delta I_z=0$.

The situation is more complex in the case of transitions between two E doublets split by the hyperfine interactions. Calling Δ_i and Δ_f the overall hyperfine splitting of the initial and final electronic levels, respectively, the presence of electric (ED) and magnetic dipole (MD) contributions at the same time [Fig. 5(b)] should give rise to the presence of 16 hyperfine lines, 8 with hyperfine splitting $\Delta_{ED}=|\Delta_i+\Delta_f|/(2I)$ and 8 with hyperfine splitting $\Delta_{MD}=|\Delta_i-\Delta_f|/(2I)$. However, a situation in which all the 16 lines are observable and well resolved is never achieved in practice, not only because one of the two contributions might be much smaller than the other, but also because of the hyperfine energy gap values. If Δ_i is much larger than Δ_f or vice versa, $|\Delta_i+\Delta_f|/|\Delta_i-\Delta_f|\simeq 1$; therefore, one would be able to observe only eight lines (each one a superposition of two unresolved transitions between hyperfine levels). On the other hand, if $\Delta_i\simeq\Delta_f$, then $|\Delta_i-\Delta_f|\simeq 0$, and a ninth line, due to the MD contribution, is observed at the center of the hyperfine structure [i.e., at the bare energy of the considered electronic transition, see Fig. 3(b)].

The effects of a second-order hyperfine interaction are also detectable in some cases. As one expects from perturbation theory, this term may have a significant effect on groups of electronic levels separated by small energy gaps. This gives rise to a contribution to the hyperfine splitting, which is proportional to I_z^2 rather than to I_z, i.e., a pseudoquadrupolar coupling with strength inversely proportional to the energy separation between the levels considered.[38] This may add to the usual first-order (Zeeman-like) hyperfine splitting if at least one E-type doublet is concerned in the process, or give rise to a pure pseudoquadrupolar splitting if two singlets, one of A1 and one of A2 type, are close enough (an A_n singlet is not connected to another A_n singlet of the same type by any matrix element). One typical example is the non-equi-spaced hyperfine pattern shown in Fig. 3(a), which is related to the transition [sketched in Fig. 5(c)] from the first excited doublet state at 12.26 cm^{-1} to the A_2 singlet at 5101.4 cm^{-1}; the latter is indeed separated by only 2.6 cm^{-1} from an A_1 singlet (see Table I, third and fifth columns). In order to take account of all these effects correctly, we calculated the energy spectra by numerically diagonalizing the full matrix representing each multiplet in the nuclear- and electronic-moment product space. No free parameters were used: the values of the free-ion and crystal-field parameters were fixed in the previous section by fitting the electronic energy-level positions, while the value $A_J=2.71\times 10^{-2}$ cm^{-1} for the hyperfine coupling constant within the ground $^5I_8$ multiplet of Ho^{3+} was directly taken from Ref. 6, and was properly scaled for all excited multiplets taking into account the values of the reduced matrix elements $\langle J\|\mathbf{N}\|J\rangle$.[7] The results of this calculation are given in Table I along with their experimental counterparts, and the agreement between the two is excellent; moreover, also the finer pseudoquadrupolar effects are well described.

The small energy gap, which (for a few lines) separates the eight hyperfine levels of a doublet into two groups of four levels each [e.g., Figs. 4(a) and 4(b)], might be attributed to a very slight distortion of the point symmetry (with respect to the ideal D_3) at Ho-occupied sites.[10] Although a quantitative analysis is impossible due to the number of parameters involved, we have performed numerical checks by assuming that a seventh CF parameter, namely, B_4^4, is allowed: the resulting splitting exactly resembles the described pattern, and the order of magnitude of B_4^4 which is required to reproduce the measured gap value in the ground state is 100 times smaller than other CF parameters [Fig. 5(d)], so that this small local distortion is negligible with respect to other possible effects.[39]

V. CONCLUSIONS

The high-resolution absorption spectra of a YAB single crystal doped with 1% m.f. Ho^{3+}, measured over wide wave number (4000–25000 cm^{-1}) and temperature (9–300 K) ranges, have been analyzed in detail, taking advantage also of theoretical calculations. Specific attention was focused on the hfs, which *decorates* many lines and makes the spectra still more complex. Thanks to the high resolution (0.01 cm^{-1}), low temperature measurements, line sharpness, and good quality of the sample, the hfs was clearly revealed for a high number of lines in a wide wave number range [up to $\simeq$21 300 cm^{-1}, see, for example, Fig. 3(d)]. hfs is detected for lines induced by many Ho^{3+} transitions, i.e., from $^5I_8$ to $^5I_7$, $^5I_6$, $^5I_5$, $^5F_5$, $^5S_2$, $^5F_4$, $^5F_3$, and $^3K_8$ manifolds, respectively. The careful analysis of the spectra in the 9–20 K range allowed us also to monitor and measure the hyperfine splitting of the first two E sublevels in the ground manifold ($^5I_8$). The spectroscopic evidence of hfs related to Ho^{3+} centers in systems such as $LiYF_4$, CaF_2, and $CsCdBr_3$ is seemingly restricted to lines originated by $^5I_8\rightarrow{}^5I_7$, $^5I_6$, and $^5F_5$ transitions, respectively.[10,12–23]

A variety of hfs patterns was monitored (see Figs. 3 and 4), which differ in the number of components, their separation, and their relative statistical weight. These features were well accounted for on the basis of the involved level symmetry, the type of transitions (electric- and magnetic-dipole allowed), the possibility of a second-order (pseudoquadrupolar) coupling between close levels, and very slight distortion of the point symmetry in Ho-occupied sites. The calculated hfs splittings are in excellent agreement with the measured ones (see Table I), confirming the correctness of the theoretical CF approach. On these favorable grounds, possible future developments for the present study could be envisaged: for example, polarized optical spectra could be used to separate the electric- and magnetic-dipole contributions[10] by exploiting the detailed selection rules.

In addition, our results also provide a thorough description and deep insight into the spectroscopic characteristics induced by Ho^{3+} in a system which is also relevant for laser applications. The Ho^{3+} transitions from the ground $^5I_8$ to the excited $^5I_7$, $^5I_6$, $^5I_5$, $^5I_4$, $^5F_5$, $^5S_2$, $^5F_4$, $^5F_3$, $^5F_2$, $^3K_8$, and $^5G_6+{}^5F_1$ manifolds were identified. The crystal-field induced splitting was evaluated with high accuracy for all manifolds. Even the position of all ground manifold sublevels could be determined (see Table I): usually this task is easily accomplished by fluorescence measurements, but not by means of

absorption. A complete energy-level scheme is supplied, providing the correct absorption line attribution. The number of observed lines is in agreement with the partial level degeneracy lifting induced by the D_3 symmetry. In spite of the spectral complexity, the experimentally determined energy levels were successfully fitted with a single-ion model and the crystal-field parameters were obtained (see Tables I and II). The theoretical assignment of level symmetry corresponds to the expected allowed transitions. The sign and order of magnitude of all CF parameters agree with those of Dy and Er in the same material and point toward a unified CF picture for YAB; the extension of this knowledge to other systems is crucial to identify good candidates for quantum manipulation and tailor their optical properties where needed.

ACKNOWLEDGMENTS

The authors are deeply indebted to Giuseppe Amoretti (Physics Department, University of Parma) for helpful suggestions and discussions, and thank C. Mora (IMEM-CNR, Parma) for technical help and V. Horváth (Research Institute for Solid State Physics and Optics, Budapest) for sample chemical analyses. The financial support from CNR-HAS project, Italian MiUR, and Hungarian Research Fund OTKA T-046481 are gratefully acknowledged. The present publication has been created also in the framework of the Hungarian and Italian intergovernmental science and technology cooperation with the support of the Research and Technology Innovation Fund and the Italian Ministry of Foreign Affairs.

*rosanna.capelletti@unipr.it

[1] A. Abragam and M. H. L. Pryce, Proc. R. Soc. London, Ser. A **205**, 135 (1951).
[2] W. J. Childs, H. Crosswhite, L. S. Goodman, and V. Pfeufer, J. Opt. Soc. Am. B **1**, 22 (1984).
[3] S. Bertaina, S. Gambarelli, A. Tkachuk, I. N. Kurkin, B. Malkin, A. Stepanov, and B. Barbara, Nat. Nanotechnol. **2**, 39 (2007).
[4] O. Guillot-Noël, Ph. Goldner, E. Antic-Fidancev, and J. L. Le Gouët, Phys. Rev. B **71**, 174409 (2005).
[5] R. Giraud, W. Wernsdorfer, A. M. Tkachuk, D. Mailly, and B. Barbara, Phys. Rev. Lett. **87**, 057203 (2001).
[6] A. Abragam and B. Bleaney, *Electron Paramagnetic Resonance of Transition Ions* (Clarendon, Oxford, 1970).
[7] In more general terms, the hyperfine interaction between the orbital electrons and the nuclear spin is given by $H_{hf}=2\mu_B\mu_N g_I \mathbf{I} \Sigma_j \mathbf{N}_j/r_j^3$, where j labels the electrons and $\mathbf{N}_j=\mathbf{l}_j-\mathbf{s}_j+3\mathbf{r}_j(\mathbf{r}_j\cdot\mathbf{s}_j)-r_j^2$. Equation (1) follows from the consideration that the matrix elements of $\mathbf{N}$ are proportional to those of $\mathbf{J}$ within a single $^{2S+1}L_J$ multiplet, A_J being, therefore, proportional to the reduced matrix element $\langle J\|\mathbf{N}\|J\rangle$.
[8] A. A. Kaminskii, *Laser Crystals*, 2nd ed. (Springer-Verlag, Berlin, 1990).
[9] G. H. Dieke, *Spectra and Energy Levels of Rare Earth Ions in Crystals* (Wiley, New York, 1968), p. 46.
[10] N. I. Agladze and M. N. Popova, Solid State Commun. **55**, 1097 (1985).
[11] I. Földvári, A. Baraldi, R. Capelletti, N. Magnani, R. Sosa F., A. Munoz F., L. A. Kappers, and A. Watterich, Opt. Mater. **29**, 688 (2007).
[12] N. I. Agladze, M. N. Popova, G. N. Zhizhin, V. J. Egorov, and M. A. Petrova, Phys. Rev. Lett. **66**, 477 (1991).
[13] R. M. Macfarlane, A. Cassanho, and R. S. Meltzer, Phys. Rev. Lett. **69**, 542 (1992).
[14] J. P. D. Martin, T. Boonyarith, and N. B. Manson, J. Lumin. **63**, 297 (1995).
[15] M. N. Popova and N. I. Agladze, Mol. Phys. **102**, 1315 (2004).
[16] J. P. D. Martin, T. Boonyarith, N. B. Manson, M. Mujaji, and G. D. Jones, J. Phys.: Condens. Matter **5**, 1333 (1993).
[17] T. Boonyarith, J. P. D. Martin, and N. B. Manson, Phys. Rev. B **47**, 14696 (1993).
[18] N. B. Manson, T. Boonyarith, and J. P. D. Martin, J. Lumin. **64**, 39 (1995).
[19] D. P. McLeod and M. F. Reid, J. Alloys Compd. **250**, 302 (1997).
[20] G. D. Jones and N. M. Strickland, J. Lumin. **102-103**, 166 (2003).
[21] J.-P. R. Wells, G. D. Jones, M. F. Reid, M. N. Popova, and E. P. Chukalina, Mol. Phys. **102**, 1367 (2004).
[22] N. M. Strickland and G. D. Jones, Mol. Phys. **102**, 1345 (2004).
[23] M. Mujaji, G. D. Jones, and R. W. G. Syme, Phys. Rev. B **48**, 710 (1993).
[24] Gy. Mészáros, E. Sváb, E. Beregi, A. Watterich, and M. Tóth, Physica B **276-278** 310 (2000).
[25] A. Baraldi, R. Capelletti, N. Magnani, M. Mazzera, E. Beregi, and I. Földvári, J. Phys.: Condens. Matter **17**, 6245 (2005).
[26] A. A. Filimonov, N. I. Leonyuk, L. B. Meissner, T. I. Timchenko, and I. S. Rez, Krist. Tech. **9**, 63 (1974).
[27] S. W. Henderson, C. P. Hale, J. R. Magee, M. J. Kavaya, and A. V. Huffaker, Opt. Lett. **16**, 773 (1991).
[28] E. V. Koporulina, N. I. Leonyuk, D. Hansen, and K. L. Bray, J. Cryst. Growth **191**, 767 (1998).
[29] A. Baraldi, I. Földvári, R. Capelletti, N. Magnani, M. Mazzera, and E. Beregi, Phys. Status Solidi C **4**, 1364 (2007).
[30] A. Baraldi, R. Capelletti, M. Mazzera, A. Ponzoni, G. Amoretti, N. Magnani, A. Toncelli, and M. Tonelli, Phys. Rev. B **72**, 075132 (2005).
[31] E. Beregi, E. Hartmann, L. Malicskó, and J. Madarász, Cryst. Res. Technol. **34**, 641 (1999).
[32] G. Dominiak-Dzik, W. Ryba-Romanowski, M. Grinberg, E. Beregi, and L. Kovács, J. Phys.: Condens. Matter **14**, 5229 (2002).
[33] I. Földvári, E. Beregi, R. Capelletti, A. Baraldi, A. Munoz, and R. Sosa, Radiat. Eff. Defects Solids **158**, 285 (2003).
[34] G. Amoretti, A. Baraldi, R. Capelletti, N. Magnani, M. Mazzera, P. Riolo, E. Sani, A. Toncelli, and M. Tonelli, Phys. Status Solidi C **2**, 248 (2005).
[35] W. T. Carnall, G. L. Goodman, K. Rajnak, and R. S. Rana, J. Chem. Phys. **90**, 3443 (1989).
[36] H. M. Crosswhite and H. Crosswhite, J. Opt. Soc. Am. B **1**, 246 (1984).
[37] B. G. Wybourne, *Spectroscopic Properties of Rare Earths* (Interscience, New York, 1965).
[38] N. I. Agladze, E. A. Vinogradov, and M. N. Popova, Sov. Phys. JETP **64**, 716 (1986).
[39] Similar results might have been obtained by choosing other symmetry-forbidden CF parameters instead of B_4^4.